

Fixed Point Laplacian Mapping: A Geometrically Correct Manifold Learning Algorithm

Anonymous Authors

Abstract—Dimensionality reduction (DR) and manifold learning (ManL) have been applied extensively in many machine learning tasks, including computer vision, image analysis and pattern recognition just to name a few. However, the geometrical correctness of DR and ManL models learning results is largely neglected. In this work, we investigate this important aspect of some widely used DR and ManL methods through the lens of the chart map function, which is the essential part of the definition of a manifold. It turns out that the mapping functions induced by these methods do not have the injectivity (i.e. one-to-one mapping) between ambient space and latent space. This poses the distinguishability problem for down-stream tasks. Without injectivity, two distinct points on a manifold may be projected to the same point in the latent space learnt by DR or ManL methods, and hence the later process cannot separate them apart, resulting in inevitable errors. To address this problem, we provide a provably correct algorithm called fixed points Laplacian mapping (FPLM), which has the geometric guarantee to find a representation of a manifold with injectivity by using a simplicial complex generated on manifold. We further discuss the property of our proposed method via various aspects, including its link to the popular graph neural networks (GNNs) and deep neural networks (DNNs). Its geometric correctness is demonstrated by extensive experimental results and theoretical proofs. Moreover, experiments also show our method is capable of evaluating the quality of simplex decomposition of the manifold and detecting manifold intrinsic dimensions for real-world datasets.

Index Terms—Manifold Learning, Chart Map, Distinguishability

I. INTRODUCTION

Dimensionality reduction (DR) and manifold learning (ManL) have been widely applied in many different domains, including computer vision [1], signal processing [2], speech recognition [3], neuroinformatics [4] and bioinformatics [5]. The usefulness comes from the well-accepted manifold assumption: *observed samples lie on a non-linear low dimensional manifold embedded in a high dimensional ambient space*. The main focus of various ManL methods is to learn the manifold structure from the sampled data along with DR to obtain the latent space representation. Many methods have been proposed in recent decades, such as the classical linear Principal Component Analysis (PCA) [6], Multi-dimensional Scaling (MDS) [7] as well as the non-linear Isomap [8], Local Linear Embedding (LLE) [9], Laplacian Eigenmap (LE) [10], Local Tangent Space Alignment (LTSA) [11] and Hessian Eigenmaps [12], among others.

a) *Geometric correctness and its implications:* Although ManL and DR methods serve as an important pre-processing step in machine learning applications, unfortunately the geometrical correctness of their learning results is rarely discussed.

Particularly, it is not clear whether the induced map from input to output is injective (i.e. one-to-one mapping), and further bijective (i.e. one-to-one and onto). The injectivity is critical to avoid ambiguity and information loss because it guarantees that a point in the manifold has its unique image in the low dimensional space. This has important implications for downstream tasks where distinguishability between points is crucial.

For example, in regression problems, if some points were mapped to a single point for being non-injective, usually called collapsing, then the representation of these points would be the same. No regressor can differentiate them and therefore the prediction would be the same, incurring inevitable prediction error. This may seem less of an issue in classification and clustering tasks where the prediction is the membership and the decision function as a whole has no injectivity. However, the true underlying function is a continuous function, e.g. probability function by softmax in many deep learning neural networks. Hence essentially it is the same as regression. Different observations from different classes/clusters may collapse and end in classification error. Rarely any learning task is immune to this problem. Even in many trending research directions, such as contrastive learning [13] and self-supervised learning [14], the learning results fundamentally rely on the representation generated by an encoder. The lack of injectivity incurs unnecessary information loss, reduces the model adequacy and compromises performance.

Nevertheless, we observed that some widely-used ManL and DR methods *fail* to produce an injective map even for the simplest 2-dimensional manifolds, such as paraboloid (see Fig. 1 and Section V). Despite being critical, the verification of injectivity is often nontrivial because most methods define the mapping implicitly through optimizing target representations in latent space. In this paper, we investigate the injectivity problems within the DR and ManL methods via the manifold chart mapping function, which is by definition (locally) bijective, as well as simplex decomposition of the manifold (defined in Section II).

b) *Observation and Motivation:* For any manifold, a chart map is a bijection between the manifold to a latent space locally. Given that ManL and DR methods claim to learn the manifold, it is vital to ensure that those learned representations are bijective or at least globally injective. For manifold with intrinsic dimension $d = 1$, the bijectivity can be ensured by order preserving, i.e. checking the order of the latent representations in \mathbb{R} . However, when $d > 1$, things become challenging since there exists no notion of ordering.

Therefore, the crux is the implementation of such ordering for any d .

Our solution to this challenge is to observe if a ManL/DR method preserves local structure. Given our sample from manifold consists mainly discrete points, a bijective map should preserve the simplicial complex/decomposition structure (mesh) of the points, which is the linear approximation of local structure of the manifold. So to test injectivity of a map, we can generate a known manifold with discrete points, derive the mesh and apply the mesh to mapped points in latent space to see if the mesh is well preserved i.e. no cross over because any overlapping of simplices indicates lack of injectivity.

Note that for unknown manifold, i.e. only discrete points observed, one can apply simplex decomposition on the sample. The simplex decomposition [15] is an advanced alternative than K nearest neighbour (KNN) graph to represent the manifold, such as surface triangulation for $d = 2$ and tetrahedralization for $d = 3$ [15]–[17]. These methods generate a piece-wise linear approximation of the manifold so that, under appropriate sampling conditions, the manifold approximation quality can be guaranteed. Given a simplex decomposition of a manifold that captures its structure, an injective mapping is required to preserve the simplex structures, including integrity, connectivity and neighbouring relations. For example, when $d = 2$, an injective map over the entire triangulation should be one-to-one over each triangle, edge, and point, with no degeneracy and intersection of triangles and edges.

Applying the above technique, we observe in Fig. 1, that Laplacian Eigenmap fails to preserve the simplex of a 2-dimensional paraboloid manifold even though we have replaced the KNN graph with adjacency matrix from the simplex decomposition (the third sub-figure from left). This suggests the map implicitly defined by LE is not injective. Similar observations have also been made (in Section V) for other commonly used ManL and DR methods.

Note that by restricting the domain of a injective mapping/function to the pre-image of its co-domain, we get bijectivity. In later discussion, we may use injective/bijective interchangeably with this in mind. Although our empirical observations suggest these methods failed in the bijectivity test for general manifold, causing potential distinguishability problems for downstream tasks, we point out that they may work for very specific type of manifolds. For example, Isomap provides a correct embedding only if the manifold itself is isometric to an open set in the latent space, and LLE only reconstructs topological balls [18]. But since the type of manifold is usually unknown, it is important to have a provably correct algorithm which guarantees bijectivity for any manifold. To address this problem, we propose a new method that is guaranteed to be bijective at least for 2-dimensional manifolds, and a certain amount of 3-manifolds¹. The theories are based upon the Tutte's planar embedding theorem [19] and its generalization [20], which states that every planar graph

¹We note that by saying d -manifold, d always standing for the intrinsic dimension of the manifold. The ambient space, where the manifold is embedded at, can be any dimension that is larger or equal than d .

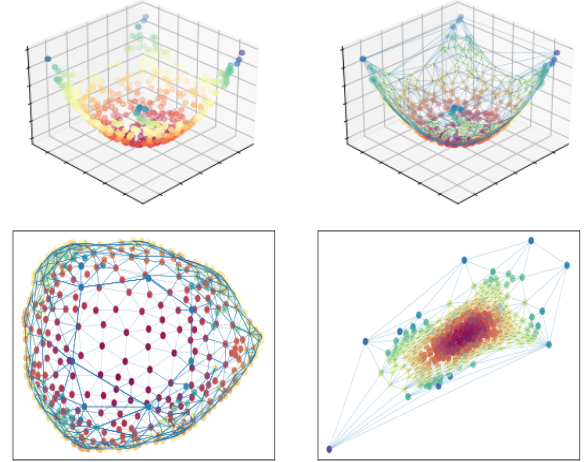


Fig. 1. Laplacian Eigenmap fails to preserve the simplex of 2-dimensional paraboloid manifold with edge intersection highlighted by thick lines. From left we have: 1. Manifold scatters, 2. Simplex decomposition of the manifold, 3. Mapping outcome after applying Laplacian Eigenmap and 4. Our proposed method that generates one-to-one correspondence between simplices (i.e., triangles).

has a convex representation embedding in \mathbb{R}^2 and with some additional conditions, a convex combination map that takes a triangulation from \mathbb{R}^2 to \mathbb{R}^2 is one-to-one. Specifically, our contributions are as follows:

- 1) We propose a method to validate the injectivity of any ManL/DR algorithm via the simplex decomposition of a manifold. By using this tool, one can check if the learning process has the weakness of collapsing.
- 2) Using this method, we identify a fundamental problem in some existing methods: the mapping function induced by these methods is not bijective, which violates the basic settings of manifolds and will cause distinguishability problems for the downstream tasks.
- 3) We offer a provably correct algorithm called fixed point Laplacian mapping (FPLM) to learn the manifold. This method has geometric guarantee to find a valid latent space representation. Further, our algorithm is applicable to any-dimensional manifolds (without genus) with structure obtained by facet-to-facet tessellation of polytopes. Furthermore, we also show the link between the proposed method with DNNs and GNNs.
- 4) Due to the geometric correctness of our algorithm, we apply our method onto the real-world dataset to illustrate the power of the algorithm in terms of evaluating the quality of manifold simplex decomposition and measuring the manifold intrinsic dimension.
- 5) By generalizing the previous embedding theorem, we make our algorithm adaptive to any non-degenerate edge-to-edge tessellation of 2-manifolds and most of 3-manifolds with and without boundary. We also discuss a sufficient condition to ensure that a mapping is always bijective to any manifold, represented by simplex decomposition.

c) *Organization*.: The remainder of the paper is organized as follows. In Section II, we introduce the basic concepts used in this paper. FPLM will be introduced in Section III with the analysis and geometric guarantees discussed in Section IV, with discussion on its properties. Section V provides the experimental results to validate our claims. Finally, the paper is concluded in Section VI with some possible extensions.

II. PRELIMINARIES

A. Manifold Structure

Consider a d -dimensional manifold \mathcal{M} (abbrev. d -manifold) embedded in \mathbb{R}^l ($l > d$) covered by a set of open sets $\mathcal{M} \subset \bigcup_{\alpha} U_{\alpha}$. For each set U_{α} , there is a homeomorphism $\psi_{\alpha} : U_{\alpha} \rightarrow \mathbb{R}^d$ (i.e. bijective, continuous and inverse is also continuous). The pair $(U_{\alpha}, \psi_{\alpha})$ forms a chart. The image of the chart map is deemed to represent the manifold structure [21]. Apart from being bijective, one can expect the chart map to preserve other geometric characteristics of manifold such as angle [22] and distance [23] when necessary. To obtain manifold local structures, one common way used in most of ManL/DR algorithms is to construct KNN graph given the observed data discretely sampled from the manifold. The estimated local structure is then used to infer the global coordinates of all data points by minimizing some loss functions. Alternatively, as discussed in Introduction section, simplex decomposition is also a good approximation to manifold and further avoids choosing the number of neighbours, a hyperparameter which is often selected arbitrarily.

Among the many developed decomposition methods, the tangential complex (TC) [24] generates piece-wise linear manifold approximation, by constructing the simplicial decomposition in tangent space. This largely reduces the complexity to the order of d , instead of l . The reconstructed manifold generated from TC, written as $\hat{\mathcal{M}}$, a simplicial complex, is topologically/geometrically isotopic to \mathcal{M} , i.e. one can continuously morph $\hat{\mathcal{M}}$ into \mathcal{M} with no self intersection.

In this paper, we assume that \mathcal{M} is an orientable connected manifold with a finite set of sample points lie on the manifold, $\mathbf{X} = \{\mathbf{x}_1, \mathbf{x}_2, \dots, \mathbf{x}_N\} \subset \mathcal{M}$, *without noise*. This is to differentiate the task of learning a bijective mapping from the manifold to its intrinsic dimension to the task of manifold reconstruction from noisy data where the latter is not within the scope of the paper. We also assume that \mathcal{M} is embedded (topologically) in the ambient space with dimension at least $d+1$ *without self-intersection*. For example, it is known that the Klein bottle in \mathbb{R}^3 is not an embedding [25], and hence will not be considered in this paper.

B. Simplex Decomposition of Manifold

A d -simplex represents a d -dimensional polytope that is the convex body formed by its $d+1$ vertices. For example, a 0,1,2-simplex stands for a point, line segment, and triangle respectively. A d -simplex is called *degenerate* if it is less than d -dimension. We will further assume that all data points sampled in \mathcal{M} are in *general position*, i.e. no colinearity among points,

or in other words, no extra point inside a simplex. For example, there will be no point inside a triangle or edge in triangulation.

Definition 1 (Simplex decomposition of \mathcal{M}). *Let \mathcal{S} be a finite set of non-degenerate d -simplex and let $D_{\mathcal{S}} = \bigcup_{S \in \mathcal{S}} S$. We call \mathcal{S} a d -simplex decomposition of \mathcal{M} if:*

- 1) *The intersection of any pair of d -simplex can either be empty or a common $\{d-1, d-2, \dots, 0\}$ simplex, and \mathbf{X} contains the vertices.*
- 2) *The boundary of $D_{\mathcal{S}}$, a closed polytope written as $\partial D_{\mathcal{S}}$, is formed by those $(d-1)$ -simplices in \mathcal{S} that are not shared.*
- 3) *$D_{\mathcal{S}}$ is homeomorphic to \mathcal{M} .*

This d -simplex decomposition of \mathcal{M} is indeed the best piecewise linear manifold approximation given a discrete sample from \mathcal{M} . Note that this differs from directly constructing simplicial complex on samples in the ambient space \mathbb{R}^l , which would result in l -simplex decomposition whose convex hull circumscribes \mathbf{X} . For 2-manifold, 2-simplex decomposition (triangulation) should be applied and tetrahedronization for $d=3$. We now take triangulation as an example to provide a few more definitions.

Let $D_{\mathcal{T}} = \bigcup_{T \in \mathcal{T}} T$ be a triangulation \mathcal{T} in \mathbb{R}^2 (T stands for a triangle). Following [20], based on the second requirement of simplex decomposition, $D_{\mathcal{T}}$ will be simply connected with boundary $\partial D_{\mathcal{T}}$. For the vertices and edges contained in the boundary $\partial D_{\mathcal{T}}$, we call them *boundary* vertices and edges, and otherwise the *interior* vertices and edges. If an edge connects two boundary vertices, we call it a *dividing edge*. For example, in figure 2, the edge $[V, W]$ is a dividing edge.

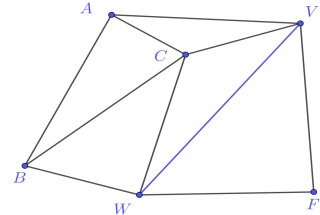


Fig. 2. Connectivity between triangles and dividing edges

Definition 2. *We say that a triangulation is strongly connected if it contains no dividing edges.*

As we mentioned in the previous sections, if a map bijectively maps the simplex decomposition to the latent space, then the connectivity between simplices must be preserved. It is easy to see that if some simplices overlap in the co-domain, the points inside the overlap region will undoubtedly have more than one pre-image, indicating a non-injective mapping.

In terms of simplex decomposition, for unknown manifold one can apply Tangential Complex algorithm [24] with required conditions and consistency test. For injectivity checking purpose for a given DR/ManL algorithm, one can use some known manifolds, for example, the graph of some function (a d -manifold embedded in \mathbb{R}^{d+1}), i.e. $(x_1, \dots, x_d, f(x_1, \dots, x_d))$,

where $x_i \in \mathbb{R}$ are latent variables and f is a continuous function; then compute the mesh (as f is known) or using TC.

III. FIXED POINT LAPLACIAN MAPPING

By using the injectivity checking method mentioned above, e.g. the example in Section I and many more in experiment section, we realize that these widely used DR/ManL methods we test are not bijective, and hence do not really learn the manifold. The question is then, is it possible to design such an algorithm which has bijectivity guarantee, at least for some manifolds? The answer is positive.

A. Settings

Based on the previous observation, one necessary condition for bijectivity is that the simplex structure in \mathcal{M} , a graph written as \mathcal{G}_S , is preserved by the mapping. Unfortunately, this is highly nontrivial. Normal neighborhood preserving and alignment ideas often seen in many DR/ManL methods do not work as they lack “hard” enforcement to ensure the preserving results, which is also the reason they fail bijectivity test. We need geometry inspired constraints and/or procedures with bijectivity embedded naturally.

We start from constructing a (weighted) adjacency matrix $\mathbf{A} \in \mathbb{R}^{N \times N}$ derived from a simplex decomposition of \mathcal{M} , with the associated degree matrix and Laplacian denoted by \mathbf{D} and \mathbf{L} .

The algorithm that we show below is a two-round procedure with the same optimization performed twice with different constraints each time. We call this algorithm fixed-point Laplacian mapping (FPLM), where the fixed points are the constraints. We denote these fixed points as $\mathbf{C} = [\mathbf{c}_1, \dots, \mathbf{c}_p]^T \in \mathbb{R}^{p \times d}$. We write $\mathbf{P}(\mathbf{C})$ as the simple polytope formed by joining fixed points in \mathbf{C} as vertices.

B. Fixed-point Laplacian Mapping (FPLM)

FPLM is formulated as follows:

$$\min_{\mathbf{Y} \in \mathbb{R}^{N \times d}} \text{tr}(\mathbf{Y}^T \mathbf{LY}), \quad \text{subject to } \mathbf{y}_i = \mathbf{c}_i, i \in [1, p] \quad (1)$$

where $\mathbf{c}_i \in \mathbb{R}^d, i \in [1, p]$ are the fixed points. We first determine whether \mathcal{G}_S is strongly connected or not (i.e., whether there is a dividing edge). If \mathcal{G}_S is strongly connected, the fixed points in the first round, collected in \mathbf{C}_1 , are the images of the vertices from a randomly selected d -simplex after reducing its dimensionality. Therefore, $\mathbf{C} = \mathbf{C}_1$ in FPLM and $p = d + 1$. Note that this step is lossless as d -simplex in \mathbb{R}^d is intrinsically d -dimensional and linear. After the first round of FPLM, the boundary of the simplex decomposition, i.e., ∂D_S , will be mapped inside $\mathbf{P}(\mathbf{C}_1)$ in \mathbb{R}^d . Recall that the boundary of a d -simplex decomposition is the $d - 1$ simplicial complex that is not shared. It is straightforward to use the boundary of the simplex decomposition as the boundary to conduct the second round of FPLM. We collect these p vertices in the boundary polytope in \mathbf{C}_2 . When \mathcal{G}_S is not strongly connected, we let n be the number of boundary vertices detected from simplex decomposition in \mathbb{R}^d , and construct a p -face ($p = n$) convex polytope in \mathbb{R}^d . One example of such convex polytope is the

regular p -face polytope. We now summarize two rounds of FPLM below.

Algorithm 1 Two Rounds of FPLM

```

1: Input: Simplex decomposition graph  $\mathcal{G}_S$ , first round fixed
   points  $\mathbf{C}_1$ .
2: Construct weighted adjacency matrix  $\mathbf{A}$  and its Laplacian
    $\mathbf{L}$  from  $\mathcal{G}_S$ .
3: if No dividing edge in  $\mathcal{G}_S$  then
4:   Obtain first-step  $\mathbf{Y}_1$  by (1) using  $\mathbf{C} = \mathbf{C}_1$ .
5: if No boundary detected inside  $\mathbf{P}(\mathbf{C}_1)$  then
6:   return  $\mathbf{Y}_1$ 
7: else
8:   Use the boundary detected as  $\mathbf{C}_2$ .
9:   Obtain second-step  $\mathbf{Y}_2$  by (1) using  $\mathbf{C} = \mathbf{C}_2$ .
10:  return  $\mathbf{Y}_2$ 
11: end if
12: else
13:   Find the number of boundary points of  $\mathcal{G}_S$  as  $p$  and
      construct a  $p$ -face convex polytope as  $\mathbf{C}_1$ .
14:   Obtain first step  $\mathbf{Y}_1$  by (1) using  $\mathbf{C} = \mathbf{C}_1$ .
15:   return  $\mathbf{Y}_1$ 
16: end if

```

IV. ANALYSIS OF ALGORITHM AND DISCUSSIONS

We here justify that the above procedure results in a bijective mapping. The line of proofs are summarized as follows. We first show that the mapping induced from FPLM is a convex combination mapping over simplex decomposition. Then taking 2-manifolds as an example, we prove that the convex combination mapping is one-to-one over the entire triangulation. Restricting the mapping to the pre-image of the co-domain, the mapping is bijective. We further prove that the procedure is applicable to any 2-manifold with structure estimated from a non-degenerate edge-to-edge tessellation of polygons. We leave the detailed proofs of our claims to Appendix A due to the page limit. Furthermore, we discuss the proposed algorithm via different aspects, including its relationship with graph neural networks (GNNs), deep neural networks (DNNs) and its limitation.

A. Analysis of the Algorithm

a) Algebraic solution of FPLM and Convex Combination Mapping: We show the optimization process of both two rounds of FPLM here. First, consider the optimization problem of FPLM in Section III-B. We set some elements in $\mathbf{Y} \in \mathbb{R}^{N \times d}$ to be fixed points $\mathbf{C} \in \mathbb{R}^{p \times d}$ ($p \geq d + 1$) and optimize the rest. Therefore, we rearrange $\mathbf{Y} = [\tilde{\mathbf{Y}}; \mathbf{C}]$ with $\tilde{\mathbf{Y}} \in \mathbb{R}^{(N-p) \times d}$ being the unknowns and

$$\mathbf{L} = \begin{bmatrix} \mathbf{L}_y & \mathbf{L}_{yc} \\ \mathbf{L}_{yc}^T & \mathbf{L}_c \end{bmatrix}$$

where $\mathbf{L}_{yc} \in \mathbb{R}^{(N-p) \times p}$. Therefore we can reformulate the problem as

$$\min_{\tilde{\mathbf{Y}} \in \mathbb{R}^{(N-p) \times d}} \text{tr}(\mathbf{C}^T \mathbf{L}_c \mathbf{C} + \tilde{\mathbf{Y}}^T \mathbf{L}_{yc} \mathbf{C} + \mathbf{C}^T \mathbf{L}_{yc}^T \tilde{\mathbf{Y}} + \tilde{\mathbf{Y}}^T \mathbf{L}_y \tilde{\mathbf{Y}})$$

This quadratic optimization problem is convex as \mathbf{L}_y is positive definite. Then by first order condition, a global minimizer $\tilde{\mathbf{Y}}^*$ exists such that

$$\mathbf{L}_y \tilde{\mathbf{Y}}^* + \mathbf{L}_{yc} \mathbf{C} = \mathbf{0}, \text{ with solution } \tilde{\mathbf{Y}}^* = -\mathbf{L}_y^{-1} \mathbf{L}_{yc} \mathbf{C}, \quad (2)$$

where \mathbf{L}_y^{-1} is the inverse of \mathbf{L}_y . Since Laplacian matrix acts as a difference operator on features, a geometric interpretation of (2) is that $\tilde{\mathbf{Y}}^*$ should have its sum of the weighted difference of its neighbours equal $\mathbf{0}$, regardless of whether they are connected to the fixed points. This is obvious after rewriting (2) by components. That is, for any $\tilde{\mathbf{y}}_i^*, i = 1, \dots, n-p$,

$$\mathbf{D}_{ii} \tilde{\mathbf{y}}_i^* - \sum_{j \in [1, n-p]} \mathbf{A}_{ij} \tilde{\mathbf{y}}_j^* - \sum_{l \in [n-p+1, n]} \mathbf{A}_{il} \mathbf{c}_l = \mathbf{0}, \quad (3)$$

where \mathbf{A}_{ij} is the weight between sample i, j and \mathbf{D}_{ii} is the degree of \mathbf{x}_i , including the fixed points. We may further simplify (3) by considering $\mathbf{Y}^* = [\tilde{\mathbf{Y}}^*; \mathbf{C}]$. That is,

$$\mathbf{y}_i^* = \sum_{j=1}^n \frac{\mathbf{A}_{ij}}{\mathbf{D}_{ii}} \mathbf{y}_j^* = \sum_{j=1}^n \lambda_{ij} \mathbf{y}_j^*, \quad \forall i = 1, \dots, n-p, \quad (4)$$

By definition of the degree matrix, we have $\sum_{j=1}^n \lambda_{ij} = 1$, $\forall i$. This shows that every optimal non-fixed point is a convex combination of points in its neighbourhood. As we mentioned earlier, the connectivity between simplices should remain the same in both image and pre-image of a bijective function over the entire simplex decomposition. Given two simplex decomposition \mathcal{S} and \mathcal{S}' of some subsets in \mathbb{R}^d , with some abuse of notation, we call a function $f : \mathcal{S} \rightarrow \mathcal{S}'$ a *piecewise linear function* if it is continuous over entire $D_{\mathcal{S}'}$ and linear over each simplex. Similarly, we have *piece-wise linear mapping* $\phi : \mathcal{G}_{\mathcal{S}} \rightarrow \mathcal{S}$ to be a mapping taking from \mathcal{M} simplex decomposition to its latent space where the simplex structure remains. A typical DR/ManL method learns ϕ such that $\mathbf{y}_i = \phi(\mathbf{x}_i)$. If ϕ satisfies (4), we call ϕ a convex combination mapping [20]. Clearly, FPLM generates a convex combination mapping over d -simplex decomposition of the manifold.

b) *Geometric Guarantees of FPLM:* We present our central theorems for the geometric guarantees of FPLM here for 2-manifolds.

Theorem 1. *For any 2-manifold without genus, the graph induced from any valid triangulation on the manifold is planar.*

The core idea for the proof (See Appendix A) is to show the graph induced from a triangulation does not contain Kuratowski subgraph K_5 and $K_{3,3}$. We now show the features of ϕ , which is the convex combination mapping induced from FPLM.

Proposition 1. *FPLM maps all non-fixed points inside the convex hull formed by the fixed points $\mathbf{P}(\mathbf{C})$.*

Proof. We only present a sketch of the proof here. If on contrary, there is a point outside the convex hull of $\mathbf{P}(\mathbf{C})$, then there must be more points outside too due to (4). For those outside points, find the one on the edge of the convex hull, then it must have more points surrounding it too. Continue this process until all non-fixed points are exhausted. The outermost one will not have a convex hull formed by its neighbors according to supporting hyperplane theorem [26] against the fact that every non-fixed point has to be convex combination of its neighbors. Therefore the assumption is incorrect. Another way to prove this is by direct observation of the minimization from FPLM. \square

By applying the conclusion from previous works [27] [20], we proved that the first round of FPLM is one-to-one over any strongly connected triangulation. We then explored the convexity of the boundary polygon of $\mathcal{G}_{\mathcal{S}}$ after the first round of FPLM and concluded the following lemma:

Lemma 1. *Given a strongly connected triangulation \mathcal{T} , $\partial D_{\mathcal{S}}$ is mapped as a convex hull after the first round of FPLM, and hence the results from algorithm 1 is one-to-one.*

The conclusion from the above Lemma is proved by virtual of Tutte's embedding theorem [19] after we show the convexity of the image of $\partial D_{\mathcal{S}}$. However, when the triangulation is not strongly connected, the first round of FPLM is no longer injective because the dividing edge will be mapped as the boundary edge of the manifold inside the selected triangle in the first round of FPLM. Therefore, we have to directly detect the boundary from $\mathcal{G}_{\mathcal{S}}$ and generate a p -side convex polygon in \mathbb{R}^2 so that all dividing edges remain inside the boundary and none of the boundary vertices are then collinear. The following theorem justifies this part in algorithm 1.

Theorem 2. *Given a triangulation \mathcal{T} with dividing edges, FPLM with fixed points \mathbf{C} as vertices of a p -side convex polygon is one-to-one, where p is the number of boundary vertices.*

The above conclusions make FPLM applicable to any 2-manifold (orientable and connected) without genus. However, when $d \geq 3$ one may need an extra condition to ensure injectivity. We discuss this in the Appendix A.

B. Discussion on FPLM

a) *FPLM as a special graph neural network(GNN):* We discuss the relationship between FPLM and the popular GNNs. Specifically, we take the most popular GNN model: graph convolutional networks (GCN) [28] which propagates graph node feature and adjacency information as:

$$\mathbf{H}^{(\ell+1)} = \sigma(\hat{\mathbf{A}} \mathbf{H}^{(\ell)} \mathbf{W}^{(\ell)}), \quad (5)$$

where $\mathbf{H}^{(\ell+1)}$ denotes the feature matrix at layer $\ell+1$ with $\mathbf{H}^{(0)} = \mathbf{X} \in \mathbb{R}^{n \times d_0}$, i.e. the input graph features, and \mathbf{W}^ℓ is the learnable feature transformation. Additionally, we let $\hat{\mathbf{A}}$ be the normalized adjacency matrix (i.e., $\hat{\mathbf{A}} = \mathbf{D}^{1/2} \tilde{\mathbf{A}} \mathbf{D}^{1/2}$) and $\tilde{\mathbf{D}}^{1/2}$ is the diagonal matrix with entries of the weighted

sum of each node of the graph (i.e., the sum of each row of $\tilde{\mathbf{A}}$), and $\tilde{\mathbf{A}} = \mathbf{A} + \mathbf{I}$. To measure the variation of node feature representation generated from GCN, one commonly applied approach is to compute the graph Dirichlet energy defined as $E(\mathbf{H}) = \frac{1}{4} \sum_{i,j} a_{ij} \|\mathbf{h}_i/\sqrt{d_i} - \mathbf{h}_j/\sqrt{d_j}\|^2 = \frac{1}{2} (\mathbf{H}^\top \hat{\mathbf{L}} \mathbf{H})$ where $\mathbf{h}_i \in \mathbb{R}^d$ is the node representation generated from GCN at specific layer. It can be shown that the training process of GCN is equivalent to minimize the graph Dirichlet energy [29], [30].² Thus a clear analogy can be made between FPLM and GCN. As one can corresponds the graph node feature (i.e., \mathbf{X}) as the coordinates of the manifold scatters and treat adjacency matrix (i.e., $\hat{\mathbf{A}}$) as a general form (crosses between simplices are allowed) of the simplex decomposition of the manifold. Thus, FPLM is a special GCN

- with input data more geometric related i.e., sampled and further embedded from an underlying manifold, with its intrinsic dimension determined by the domain knowledge
- propagate adjacency (generated from the simplex decomposition) and manifold scatters (coordinate) information with boundary condition i.e., fixed point.
- has guarantee to produce an one-to-one correspondence between the input node features and its latent embeddings.

In fact, one can consider the FPLM problem presented in (1) as solving the Laplacian equation with boundary conditions, that is:

$$\mathbf{L}g(\mathbf{X}) = 0, \quad \text{subject to } g(\mathbf{x}_i) = \mathbf{c}_i, i \in [1, p], \quad (6)$$

in which we solve the form of $g \in \mathbb{R}^D \rightarrow \mathbb{R}^d$ to map the manifold scatters to the latent space. In fact, FPLM works for those so-called *planar* graphs (Please refer to the Appendix A for more details). Under the planer graph setting, based on our proof on the property of FPLM, we see that the *piece-wise linear mapping* ϕ we mentioned in section IV is one of solutions (as the boundary condition can vary) of g that is trained in GCN with bijective property between node representations. When the input graph is not *planar*, the problem in (6) can be utilized for graph labelling since one can write the form of function $g(\mathbf{x}_i) = (g_1(\mathbf{x}_i), g_2(\mathbf{x}_i) \dots g_d(\mathbf{x}_i))$ and the label decision for a vertex $\mathbf{x}_i \in \mathbb{R}^d$ is determined by the largest component of $g(\mathbf{x}_i)$ that is:

$$\mathcal{K}(\mathbf{x}_i) = \arg \max_{j \in \{1 \dots d\}} \{g_j(\mathbf{x})\}, \quad (7)$$

where we denote \mathcal{K} as the labelling operator. We note that once we replace the boundary condition in (6) with the fixed labels, we recover the Laplacian learning developed in [31]. This equation directly suggests that even for the real-world graph datasets which are normally not planar, the learning outcome FPLM (with a slightly modification on the format boundary condition) can be utilized for graph labelling.

²To see this, one can rewrite the propagation rule in GCN (i.e., (5) as an (Dirichlet) energy regularization problem, that is: $\mathbf{H} = \arg \min_{\mathbf{H}} \left\{ \mu \|\mathbf{X} - \mathbf{H}\|_F^2 + \frac{1}{2} \text{tr}(\mathbf{H}^\top \hat{\mathbf{L}} \mathbf{H}) \right\}$. Clearly we see the solution of this problem is the one which minimize the graph Dirichlet energy.

b) *Link to Deep Neural Networks (DNNs)*: We discuss the link between FPLM and DNNs which has been proved to be an universal approximator to any Borel measurable function [32]. For the compactness of our subsequent discussion, we define the feed-forward DNN as follows:

Definition 3 (ReLU DNN [33]). *For any number of hidden layers $\ell \in \mathbb{N}$, input and output dimensions $w_0, w_{k+1} \in \mathbb{N}$, a $\mathbb{R}^{w_0} \rightarrow \mathbb{R}^{w_{\ell+1}}$ RELU DNN is given by specifying a sequence of k nature numbers w_1, w_2, \dots, w_ℓ representing the widths of hidden layers, a set of k affine transformations $T_i : \mathbb{R}^{w_{i-1}} \rightarrow \mathbb{R}^{w_i}$ and a linear transformation $T_{\ell+1} : \mathbb{R}^{w_\ell} \rightarrow \mathbb{R}^{w_{\ell+1}}$ correspondent to the weights of hidden layers. The network induced function $f : \mathbb{R}^{n_1} \rightarrow \mathbb{R}^{n_2}$ has the form:*

$$f = T_{\ell+1} \circ \sigma \circ T_\ell \dots \circ T_2 \circ \sigma \circ T_1,$$

where \circ denote as the function composition, σ is the activation function. The **width** of the network is $\max\{w_1 \dots w_\ell\}$, and the **depth** of the network is $\ell + 1$.

Recall that we denote \mathcal{S} be the set of all simplices generated from the simplex decomposition algorithm, and FPLM induced a *piece-wise linear* map over all the elements of \mathcal{S} . Suppose \mathcal{M} is bounded by $[-B, B]^D$, and we further assume that the probability density of data distribution is positive over $[-B, B]^D$, for any piece-wise linear function $f : [-B, B]^D \rightarrow \mathbb{R}^d$ ($d \geq 1$) that support on \mathcal{S} , we have the following lemma:

Lemma 2 ([34]). *Suppose $f : [-B, B]^D \rightarrow \mathbb{R}^d$ that takes \mathcal{S} support on \mathcal{S} is with the form:*

$$f(\mathbf{x}) = \begin{cases} \mathbf{a}^T \mathbf{x} + \mathbf{b} & \text{if } \mathbf{x} \in \mathcal{S} \\ 0 & \text{otherwise} \end{cases} \quad (8)$$

then for any $\delta > 0$, there exist a neural network \mathbf{N} of width $\mathcal{O}[D(D+1)(2^D - 1)]$ and depth $2D + 1$ satisfying:

$$m(\{\mathbf{x} | f(\mathbf{x}) \neq \mathbf{N}(\mathbf{x})\}) < \delta, \quad (9)$$

where $m(\cdot)$ is the standard measure in $[-B, B]^D$.

One can easily check that the convex combination mapping ϕ induced from FPLM satisfies the property mentioned in lemma 2 mentioned above. As piecewise linear function (induced from FPLM) over a simplicial complex can be decomposed into linear functions over a simplex. Thus, we can design a network $\mathbf{N}(\mathbf{x}) \forall x \in \mathcal{S}$ concurrently to obtain a so-called meta-network $\mathbf{M}(\mathbf{x})$ as:

$$\mathbf{M}(\mathbf{x}) = \sum_{k=1}^K \mathbf{N}^{(k)}(\mathbf{x}),$$

where $\mathbf{N}^{(k)}(\mathbf{x})$ represents the linear function over the k -th simplex and K is the number of simplices the support f , therefore \mathbf{H} is of width $\mathcal{O}[D(D+1)(2^D - 1)K]$ and depth $D + 1$.

c) Limitation in Higher Dimensional Manifold Mesh:

It has been reported that convex combination may not be one-to-one if $d \geq 3$. A counter-example has been reported in [35]. However, in that particular counter-example, they created one point within a facet of a tetrahedron conflicting with our assumption on the discrete sample on manifold, i.e. all points are assumed in general position. Hence, this counter-example does not apply. We further point out that orientation preserving (OP) is necessary for an algorithm with its induced mapping to be bijective for any d -simplex decomposition [36]. Based on the conclusion from [20], we easily derive that FPLM is both local/global OP for connected orientable 2-manifolds due to its established bijectivity over triangulation. However, when $d \geq 3$, the proof of OP in FPLM is still wanted.

V. EXPERIMENTS

In this section, we first investigate the learning performance of widely used state-of-the-art DR/ManL algorithms. The structure of every 2-manifold was generated by applying either Tangential Complex (TC) algorithm [24] or Delaunary/Surface triangulation. The structure of 3-manifold is generated by using Delaunay tetrahedralization algorithm [37] included in Tetgen and TC. To have a fair comparison between FPLM and other prominent methods, the adjacency information obtained from the simplex decomposition will be used as the input as manifold structure. The number of the line segments crosses will be counted as a measure to evaluate the learning performance for all included models. Secondly, we apply FPLM onto the real world dataset (MNIST [38]) to show the power of FPLM of evaluating the tangential mesh quality and detecting the manifold intrinsic dimension.

A. FPLM on 2-manifolds

Experiment setup. The 2-manifolds included in the experiment are: Monkey saddle, Swiss roll, Paraboloid, Twin peaks and Sphere. We construct a weighted adjacency matrix from triangulation via rbf kernel function. That is, $A_{ij} = \exp(-\gamma d_m(\mathbf{x}_i, \mathbf{x}_j))$ if \mathbf{x}_i is connected to \mathbf{x}_j , where we use l_2 distance $d_m(\mathbf{x}, \mathbf{y}) = \sqrt{\sum_{i=1}^d (x_i - y_i)^2}$ for $\mathbf{x}, \mathbf{y} \in \mathbb{R}^d$. For all experiments, we fix $\gamma = 0.1$.

The settings of other learning algorithms are as follows: for LE and LTSA, we use pre-computed \mathbf{A} as input; for Local Linear Embedding, we use adjacency matrix constructed from the simplex decomposed graph as input to replace the neighborhood graph; for Isomap, we construct the distance matrix from the simplex decomposed graph and distance; for MDS and tSNE, we use default settings. Finally, for Manifold Autoencoder, we construct a neural network with layer $3 \times 64 \times 2 \times 64 \times 3$. Activation function is Relu; dropout layer is considered with $p = 0.2$. Batch normalization is applied to the bottleneck layer. The optimizer is chosen to be ADAM with a learning rate of 0.1. For every experiment, we run 1000 epochs. All experiments are carried out on a laptop computer running on a 64-bit operating system with Intel Core i5-8350U 1.90GHz CPU and 16G RAM with Python 3.36.

For the manifold with boundary, the second round output of FPLM will be compared with other learning algorithms. Due to the space limit, we will only present the investigation results of swiss roll in Fig. 3 and 4. For the rest of the result, please see Appendix D. As we can see, all results in Fig. 4 are with line crosses, indicating that the connectivity between triangles is not preserved; thus the mapping induced from these methods is not one-to-one.

B. FPLM on 3-manifolds

To show the learning performance of FPLM on any given tetrahedron mesh, we use both Delaunay tetrahedralization algorithm described in Tetgen [37] and TC to create tetrahedral meshes in \mathbb{R}^3 . Given that all the d -manifolds we considered in this paper can at least be embedded into \mathbb{R}^{d+1} ; hence the points that we simulated in the manifold latent space can always be embedded in at least \mathbb{R}^4 without self-intersection. Note that the boundary of tetrahedral mesh can be detected as the 2-simplex that is not shared in tetrahedral mesh. Due to the variety of embedding functions from \mathbb{R}^3 to \mathbb{R}^4 , the boundary detect from \mathbb{R}^3 will be, in general, different from the boundary of the manifold in \mathbb{R}^4 or higher. Moreover, for the first round of FPLM, the fixed points will be the vertices of randomly selected tetrahedral; for the second round of FPLM, the fixed points will be the vertices of the polytope directly detected from tetrahedralization mesh. Fig 5 shows FPLM results on tetrahedral mesh of the famous "Delaunay Example" in Python Vista [39].

By counting the number of intersections between the planes formed by the faces (triangles) of tetrahedrons (In the last sub-figure in Figure 5), we found that the result generated from FPLM perfectly preserved the structure of the manifold, since all planes are only intersect with either a common edge, or point. In addition, to show a better visualization result, we plot a subset of the tetrahedralization result by visualizing the tetrahedron below the (x, y) plane. The FPLM process, however, will still conduct using the entire dataset. By direct observation, we can see FPLM preserves the structure of tetrahedralization result.

C. Mesh Quality Measurement and Intrinsic Dimension Detection

Due to the geometric validity of the algorithm, FPLM naturally equips with the power to measure the quality of mesh utilized for manifold reconstruction (i.e., TC) in the ambient space, for example images. As it is not possible to directly check whether the mesh on the manifold satisfies the features of simplex decomposition in definition 1 in high dimensional ambient space, in this experiment we apply FPLM to the MNIST data to show the quality of the simplex decomposition of manifold in a **visible** dimension (i.e. \mathbb{R}^2). The simplex decomposition of 500 randomly selected MNIST hand-written digits was generated using tangential complex,

From the Figure 6 we show large number of edge crosses from all learning results. However, due to the geometric correctness of FPLM, **only** the learning result from FPLM is

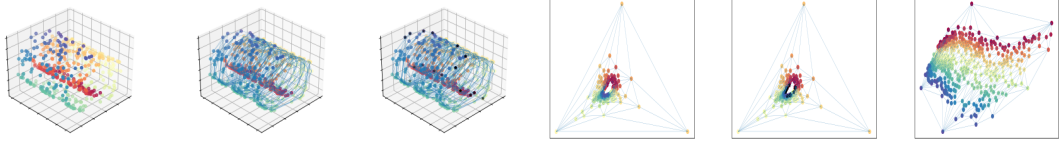


Fig. 3. FPLM on Swiss roll: from left (a) Manifold scatters,(b) Triangulation on manifold, (c) Boundary detection (d) First round FPLM, (e) Boundary detection for the first round FPLM, (f) Final result.

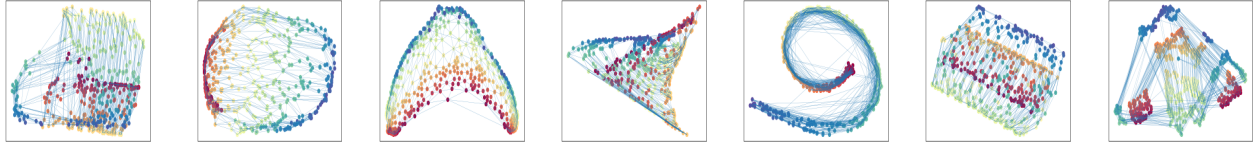


Fig. 4. Other methods on Swiss roll with number of crosses. From left, (a) AE: 4585 crosses,(b) Isomap: 1942 crosses, (c) LE:937 crosses, (d) LLE: 3623 cross, (e)LTSA: 36773 crosses, (f) MDS: 3804 crosses, (g) t-SNE: 10088 crosses

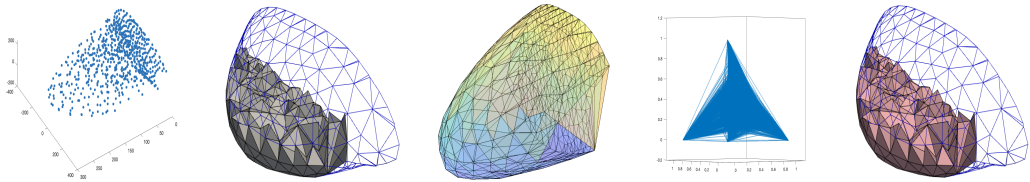


Fig. 5. FPLM on tetrahedron mesh example. (a). Point scatter (b). tetrahedralization (c). Boundary detection (d). First round FPLM (e). Second round FPLM

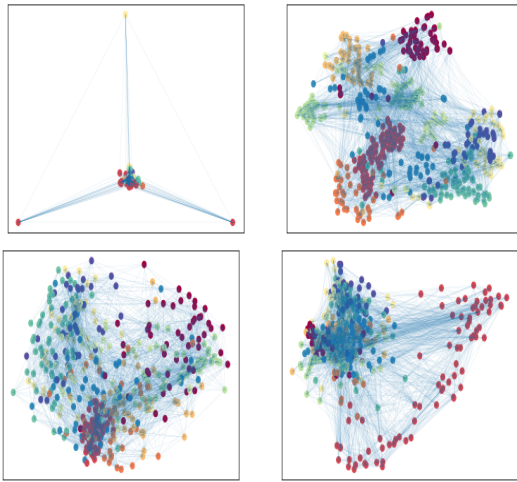


Fig. 6. Simplex Decomposition Quality Evaluation on MNIST Dataset: (a)FPLM (79610 crosses) (b).TSNE (657223 crosses) (c). Isomap (515837 crosses) (d). Local Linear Embedding (935172 crosses)

capable of producing a valid quality evaluation of the simplex decomposition generated in the high dimensional space. The large number of edge crosses detected from FPLM indicates that there must be several simplices with their edges crossed with each other in the high dimensional space. The underlying reasons of causing this imperfect manifold intrinsic mesh vary between computational geometry algorithms. One of the most classic reasons is regarded to the local feature size [24] which can be intuitively defined as how many data points that

one simplex decomposition algorithm requires to construct a manifold local patch using d -simplices. As most of the simplex decomposition methods rely on a local tangent space estimation of the manifold, when the manifold observation is locally sparse, inconsistent tangential simplices are more likely to be generated and eventually result as the edge crosses in FPLM results. This anomaly detected from the FPLM outputs is align with the notion of inconsistency mentioned in [24], implying wide range of functionalities of FPLM. Another main reason of causing low quality of simplex decomposition is the estimate of manifold intrinsic dimension, there are numbers of researches [40] [41] [42] published in the recent years showing different dimension estimation results of the manifold in MNIST datasets. Hence it may not be appropriate for representing manifold structure in MNIST by using 2-simplex decomposition, and this align with our observations of the FPLM outputs.

VI. CONCLUSION

This paper explores the injectivity of some most widely used dimensionality reduction algorithms by proposing a method for this purpose. To our surprise, these methods do not have injectivity for manifolds we tested. This arouses distinguishability problem in down-streaming tasks bringing inevitable errors. To address this issue, we developed the two-round FPLM, with the geometric guarantee of bijectivity in its induced map under some conditions. This was proven by theoretic analysis on 2-manifolds. Furthermore, our experimental results supported this finding for 2-manifolds and some 3-manifolds. A future study is to investigate if this procedure has injectivity/bijectivity for manifolds with arbitrary dimensions.

REFERENCES

- [1] R. Hadsell, S. Chopra, and Y. LeCun, "Dimensionality reduction by learning an invariant mapping," in *2006 IEEE Computer Society Conference on Computer Vision and Pattern Recognition (CVPR'06)*, vol. 2. IEEE, 2006, pp. 1735–1742.
- [2] L. Rui, H. Nejati, and N.-M. Cheung, "Dimensionality reduction of brain imaging data using graph signal processing," in *2016 IEEE International Conference on Image Processing (ICIP)*. IEEE, 2016, pp. 1329–1333.
- [3] L. Van Der Maaten, E. Postma, and J. Van den Herik, "Dimensionality reduction: a comparative," *J Mach Learn Res*, vol. 10, no. 66-71, p. 13, 2009.
- [4] B. Mwangi, T. S. Tian, and J. C. Soares, "A review of feature reduction techniques in neuroimaging," *Neuroinformatics*, vol. 12, no. 2, pp. 229–244, 2014.
- [5] Q. Zou, J. Zeng, L. Cao, and R. Ji, "A novel features ranking metric with application to scalable visual and bioinformatics data classification," *Neurocomputing*, vol. 173, pp. 346–354, 2016.
- [6] S. Wold, K. Esbensen, and P. Geladi, "Principal component analysis," *Chemometrics and intelligent laboratory systems*, vol. 2, no. 1-3, pp. 37–52, 1987.
- [7] M. A. Cox and T. F. Cox, "Multidimensional scaling," in *Handbook of data visualization*. Springer, 2008, pp. 315–347.
- [8] M. Balasubramanian, E. L. Schwartz, J. B. Tenenbaum, V. de Silva, and J. C. Langford, "The isomap algorithm and topological stability," *Science*, vol. 295, no. 5552, pp. 7–7, 2002.
- [9] S. T. Roweis and L. K. Saul, "Nonlinear dimensionality reduction by locally linear embedding," *science*, vol. 290, no. 5500, pp. 2323–2326, 2000.
- [10] M. Belkin and P. Niyogi, "Laplacian eigenmaps for dimensionality reduction and data representation," *Neural computation*, vol. 15, no. 6, pp. 1373–1396, 2003.
- [11] Z. Zhang and H. Zha, "Principal manifolds and nonlinear dimensionality reduction via tangent space alignment," *SIAM journal on scientific computing*, vol. 26, no. 1, pp. 313–338, 2004.
- [12] D. L. Donoho and C. Grimes, "Hessian eigenmaps: Locally linear embedding techniques for high-dimensional data," *Proceedings of the National Academy of Sciences*, vol. 100, no. 10, pp. 5591–5596, 2003.
- [13] P. Khosla, P. Teterwak, C. Wang, A. Sarna, Y. Tian, P. Isola, A. Maschinot, C. Liu, and D. Krishnan, "Supervised contrastive learning," *arXiv preprint arXiv:2004.11362*, 2020.
- [14] L. Jing and Y. Tian, "Self-supervised visual feature learning with deep neural networks: A survey," *IEEE Transactions on Pattern Analysis and Machine Intelligence*, 2020.
- [15] J.-D. Boissonnat, R. Dyer, and A. Ghosh, "Delaunay triangulation of manifolds," *Foundations of Computational Mathematics*, vol. 18, no. 2, pp. 399–431, 2018.
- [16] F. Cazals and J. Giesen, "Delaunay triangulation based surface reconstruction," in *Effective computational geometry for curves and surfaces*. Springer, 2006, pp. 231–276.
- [17] A. Maglo, C. Courbet, P. Alliez, and C. Hudelot, "Progressive compression of manifold polygon meshes," *Computers & Graphics*, vol. 36, no. 5, pp. 349–359, 2012.
- [18] J. Chen and Y. Liu, "Locally linear embedding: a survey," *Artificial Intelligence Review*, vol. 36, no. 1, pp. 29–48, 2011.
- [19] W. T. Tutte, "How to draw a graph," *Proceedings of the London Mathematical Society*, vol. 3, no. 1, pp. 743–767, 1963.
- [20] M. Floater, "One-to-one piecewise linear mappings over triangulations," *Mathematics of Computation*, vol. 72, no. 242, pp. 685–696, 2003.
- [21] V. Guillemin and A. Pollack, *Differential topology*. American Mathematical Soc., 2010, vol. 370.
- [22] R. Courant, *Dirichlet's principle, conformal mapping, and minimal surfaces*. Courier Corporation, 2005.
- [23] A. M. MacEachren and J. V. Davidson, "Sampling and isometric mapping of continuous geographic surfaces," *The American Cartographer*, vol. 14, no. 4, pp. 299–320, 1987.
- [24] J.-D. Boissonnat and A. Ghosh, "Manifold reconstruction using tangential delaunay complexes," *Discrete & Computational Geometry*, vol. 51, no. 1, pp. 221–267, 2014.
- [25] H. Whitney, "The singularities of a smooth n-manifold in (2n-1)-space," *Annals of Mathematics*, pp. 247–293, 1944.
- [26] S. Boyd, S. P. Boyd, and L. Vandenberghe, *Convex optimization*. Cambridge university press, 2004.
- [27] H. Kneser, "Losung der aufgabe 41," *Jahresber. Deutsche Meth.*, pp. 123–124, 1926.
- [28] T. N. Kipf and M. Welling, "Semi-supervised classification with graph convolutional networks," *arXiv:1609.02907*, 2016.
- [29] F. Wu, A. Souza, T. Zhang, C. Fifty, T. Yu, and K. Weinberger, "Simplifying graph convolutional networks," in *International Conference on Machine Learning*. PMLR, 2019, pp. 6861–6871.
- [30] Y. Wang, Y. Wang, J. Yang, and Z. Lin, "Dissecting the diffusion process in linear graph convolutional networks," *Advances in Neural Information Processing Systems*, vol. 34, pp. 5758–5769, 2021.
- [31] X. Zhu, Z. Ghahramani, and J. D. Lafferty, "Semi-supervised learning using gaussian fields and harmonic functions," in *Proceedings of the 20th International conference on Machine learning (ICML-03)*, 2003, pp. 912–919.
- [32] Y. Lu and J. Lu, "A universal approximation theorem of deep neural networks for expressing probability distributions," *Advances in neural information processing systems*, vol. 33, pp. 3094–3105, 2020.
- [33] R. Arora, A. Basu, P. Mianjy, and A. Mukherjee, "Understanding deep neural networks with rectified linear units," *arXiv preprint arXiv:1611.01491*, 2016.
- [34] F.-L. Fan, R. Lai, and G. Wang, "Quasi-equivalence of width and depth of neural networks," *arXiv preprint arXiv:2002.02515*, 2020.
- [35] M. S. Floater and V. Pham-Trong, "Convex combination maps over triangulations, tilings, and tetrahedral meshes," *Advances in Computational Mathematics*, vol. 25, no. 4, pp. 347–356, 2006.
- [36] Y. Lipman, "Bijective mappings of meshes with boundary and the degree in mesh processing," *SIAM Journal on Imaging Sciences*, vol. 7, no. 2, pp. 1263–1283, 2014.
- [37] H. Si, "Tetgen, a delaunay-based quality tetrahedral mesh generator," *ACM Transactions on Mathematical Software (TOMS)*, vol. 41, no. 2, pp. 1–36, 2015.
- [38] Y. LeCun, L. Bottou, Y. Bengio, and P. Haffner, "Gradient-based learning applied to document recognition," *Proceedings of the IEEE*, vol. 86, no. 11, pp. 2278–2324, 1998.
- [39] C. B. Sullivan and A. A. Kaszynski, "Pyvista: 3d plotting and mesh analysis through a streamlined interface for the visualization toolkit (vtk)," *Journal of Open Source Software*, vol. 4, no. 37, p. 1450, 2019.
- [40] V. Erba, M. Gherardi, and P. Rotondo, "Intrinsic dimension estimation for locally undersampled data," *Scientific reports*, vol. 9, no. 1, pp. 1–9, 2019.
- [41] L. Amsaleg, O. Chelly, T. Furion, S. Girard, M. E. Houle, K.-i. Kawarabayashi, and M. Nett, "Estimating local intrinsic dimensionality," in *Proceedings of the 21th ACM SIGKDD International Conference on Knowledge Discovery and Data Mining*, 2015, pp. 29–38.
- [42] T. Birdal, A. Lou, L. J. Guibas, and U. Simsekli, "Intrinsic dimension, persistent homology and generalization in neural networks," *Advances in Neural Information Processing Systems*, vol. 34, 2021.
- [43] C. Kuratowski, "Sur le probleme des courbes gauches en topologie," *Fundamenta mathematicae*, vol. 15, no. 1, pp. 271–283, 1930.
- [44] J. R. Munkres, *Elements of algebraic topology*. CRC press, 2018.
- [45] D. Freedman, "Efficient simplicial reconstructions of manifolds from their samples," *IEEE transactions on pattern analysis and machine intelligence*, vol. 24, no. 10, pp. 1349–1357, 2002.
- [46] J. Flötotto, "A coordinate system associated to a point cloud issued from a manifold: definition, properties and applications," Ph.D. dissertation, Université Nice Sophia Antipolis, 2003.
- [47] P. L. George, F. Hecht, and É. Saltel, "Automatic mesh generator with specified boundary," *Computer methods in applied mechanics and engineering*, vol. 92, no. 3, pp. 269–288, 1991.
- [48] J. Ruppert, "A delaunay refinement algorithm for quality 2-dimensional mesh generation," *Journal of algorithms*, vol. 18, no. 3, pp. 548–585, 1995.

APPENDIX

In this Appendix one, we first prove that the graph from the triangulation on 2-manifold is planar; then we show that the constraints that we assign to each round of FPLM can ensure that FPLM is one-to-one over entire triangulation. We also show that FPLM can be used for any edge-to-edge tessellation of polygons on 2-manifolds. For arbitrary dimensional manifold, we discuss sufficient conditions for bijectivity. Unfortunately, computational methods on discrete data sampled from manifold with orientation preserving is still an open question in mathematics.

A. Planarity

Given a triangulation on \mathcal{M} , we denote $G(V, E)$ as the graph containing the adjacency information of vertices and edges from \mathcal{T} . For any vertex v in G , we denote $N_v^{\mathcal{T}}$ as the vertices set that contains v 's neighboring vertices directly connected to v in \mathcal{T} . We also denote $E_v^{\mathcal{T}}$ as the set contains all the edges of v as starting/ending point. Based on the second feature of simplex decomposition in definition 1, we denote the boundary of manifold $\partial\mathcal{M}$ (from triangulation) as those edges that are only contained in one triangle. In this section, we will demonstrate that the graph induced from triangulation on \mathcal{M} is planar that can be reduced into a subset of plane so that edges will only intersect at their endpoints. We now define planar graph by stating Kuratowski's theorem [43]:

Theorem 3 (Planar Graph,Kuratowski). *A finite graph is planar if and only if it does not contain a sub-graph of the complete graph K_5 or the complete bipartite graph $K_{3,3}$ (utility graph).*

We say a graph is complete if the graph is a simple undirected graph in which a unique edge connects every pair of distinct vertices. Figure 7(a) shows a complete graph of five vertices K_5 . We say a graph is a complete bipartite graph if there are two sets of vertices U and V and every vertex of the first set is connected to every vertex of the second set. Figure 7(b) shows a complete bipartite graph ($K_{3,3}$) in which each vertex set contains 3 vertices.

B. Planarity of the graph induced from triangulation

Proposition 2. *For a triangulation on a 2-manifold in \mathbb{R}^l , there is no Kuratowski sub-graph K_5 .*

Proof. The proof is by contradiction. Assume there is K_5 . By the definition of triangulation on manifold, the intersection of any pair of triangles is either empty, a common vertex, or a common edge. However, a K_5 in \mathbb{R}^2 has two triangles intersecting with their edges of them. For example, in Figure 7 (a) The intersection of triangle $T[A,B,D]$ and triangle $T[A,B,C]$ is line segment $[A,B]$ while their edges $[A,C]$ and $[B,D]$, intersects, contradicting the condition of triangulation on 2-manifold.

Furthermore, as the triangulation on the manifold is conducted on \mathbb{R}^l (for example $l = 3$), it is possible to have the situation that one of K_5 's vertices is lifted up in another dimension so that the entire K_5 in \mathbb{R}^3 becomes a pyramid

shown in Figure 8 below. However, from the definition of triangulation, all edges can only be shared by at most once. From the figure below, it is clear to see that edge $[C,D]$ is shared by triangle $T[B,C,D]$, $T[A,C,D], T[E,C,D]$, and that contradicts to the definition of triangulation. \square

Proposition 3. *For a triangulation on 2-manifold in \mathbb{R}^l , there is no Kuratowski sub-graph $K_{3,3}$.*

Proof. The proof is also done by contradiction. Assume there is $K_{3,3}$. If $l = 2$, the result is trivial as shown in Figur 7(b): $K_{3,3}$ in \mathbb{R}^2 is always with line-segment cross, and that is contradict to our definition of triangulation.

If $l > 2$, we have the situation shown in Figur 9, in which all vertices are in \mathbb{R}^l . Observe that there is no line-cross (edge intersection) contained in this high-dimensional $K_{3,3}$. However, the plane define by the vertices $[F, A, B]$ intersects the plane defined by vertices $[A, B, E]$ at line-segment $[A, B]$, indicating self-intersection of the manifold due to the fact that the simplex decomposition is homeomorphic to \mathcal{M} . Thus the manifold that contains such feature can only be immersed to \mathbb{R}^l but not embedded. That leads to a contradiction to our basic assumption to 2-manifold being proper embedding. \square

Applying propositions 2 and 3 with theorem 3 leads the claim in Theorem 1.

From Kuratowski theorem, the triangulation \mathcal{T} on \mathcal{M} with the above features induces a *planar straight line graph*. Note that the triangulation we discuss can be the results from any triangulation outputs such as surface triangulation and tangential complex.

Remark 1 (Manifold without boundary). *For some manifolds without boundary, e.g. two sphere S^2 , it is well known that we can not map the entire manifold on the plane. One can only discretely sample from the underlying manifold and hence leave with many “oles” in the manifold. In other words, what we observed is not the entire sphere but a measure-less subset of it. Thus, it is reasonable to randomly select a triangle from this triangulation as the boundary of a “new” manifold without it, which is almost the same as S^2 but with the missing triangle. Figure 10below shows a triangle selected whose boundary serves as the boundary of this new manifold for the sampled points. There is no information loss as we know what we have taken away.*

C. Piece-wise linear mapping of FPLM

As we mentioned earlier, the connectivity between simplices formed on manifold should remain the same in both image and pre-image of a bijective function over the entire simplex decomposition. We let the image set of the chart map as $\mathbf{Z} = \{\mathbf{z}_1, \mathbf{z}_2, \dots, \mathbf{z}_N\} \in \mathbb{R}^d$. The exact position of every point in \mathbf{Z} is unknown; however, from the bijectivity of the chart map, we know that \mathbf{Z} perfectly preserves the connectivity between simplices. This means if we repeat the graph in \mathbf{Z} using the

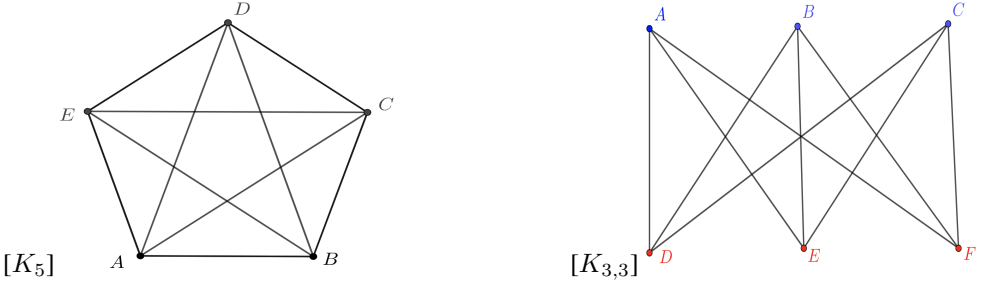


Fig. 7. Kuratowski subgraph K_5 and $K_{3,3}$

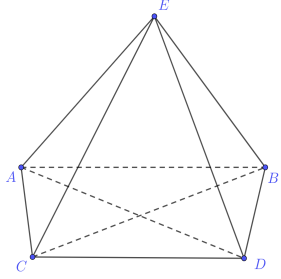


Fig. 8. Sub-graph of K_5 in \mathbb{R}^3

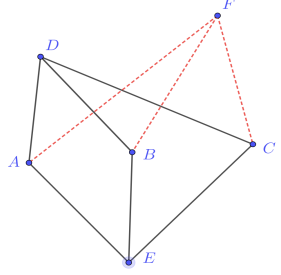


Fig. 9. Sub-graph of $K_{3,3}$ in \mathbb{R}^3

adjacency information from the simplex decomposition (\mathcal{S}) on \mathcal{M} , the integrity, connectivity, and neighboring relations between simplices will remain unchanged. We write the simplex decomposition in \mathbb{R}^d as \mathcal{S}' although it is the same as \mathcal{S} . Then for the points in both \mathcal{S} and \mathcal{S}' , they are linearly related, e.g. the weights on the edges, which is apparent in equation (4) equal to $\frac{A_{ij}}{D_{ii}}$.

We will use $N_{\mathbf{z}_i}^{S'}$ to denote the set of neighbors of \mathbf{z}_i in S' . From equation (4), the solution of FPLM is obtained by solving a system of linear equations. From equation (4) we know that each interior vertex \mathbf{y}_i^* is a convex combination of its neighbors, well aligned with the convex combination function defined as follows:

Definition 4 (Convex Combination function). *For every interior vertex \mathbf{z}_i of a simplex decomposition \mathcal{S}' in \mathbb{R}^d and $\lambda_{ij} \geq 0$, for $N_{\mathbf{z}_i}^{S'}$, if a piece-wise linear function $f : D_{\mathcal{S}'} \rightarrow \mathbb{R}$ satisfies:*

$$\sum_{\mathbf{z}_j \in N_{\mathbf{z}_i}^{S'}} \lambda_{ij} = 1 \quad (10)$$

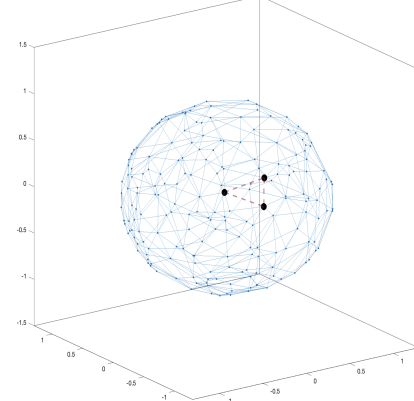


Fig. 10. Boundary triangle for a triangulation of the subset of 2D-sphere

and

$$f(\mathbf{z}_i) = \sum_{\mathbf{z}_j \in N_{\mathbf{z}_i}^{S'}} \lambda_{ij} f(\mathbf{z}_j) \quad (11)$$

Then we call f a convex combination function

Similarly, we will have piece-wise linear mapping $\phi : D_{\mathcal{S}'} \rightarrow \mathbb{R}^d$ to be any mapping that $\phi = (f_1, \dots, f_d)$ in which f_i 's are the piece-wise linear function act on each coordinate component of a given vertex \mathbf{z}_i . We call ϕ a convex combination mapping given a set of fixed non-negative weights λ_{ij} for the neighbours $N_{\mathbf{z}_i}^{S'}$ of each interior vertices $\mathbf{z}_i \in \mathcal{Z}$. We have:

$$\mathbf{y}_i^* = \phi(\mathbf{z}_i) = \sum_{\mathbf{z}_j \in N_{\mathbf{z}_i}^{S'}} \lambda_{ij} \phi(\mathbf{z}_j) \quad (12)$$

The convex combination mapping linearly adjusts the coordinates of each interior vertex in \mathcal{S}' so that for each vertex, the mapping result $\phi(\mathbf{z})$ lies in the convex hull formed by its neighbors. It is clear that \mathbf{Y}^* , the optimizer of FPLM, satisfies (12). For the rest of the paper, we write ϕ_1 for the convex combination mapping for the first round of FPLM, similarly, ϕ_2 for the second round of FPLM.

Remark 2. Together with the chart map ψ , we now summarize the whole process of Algorithm 1. If \mathcal{M} is a manifold without boundary as required, then the whole process of FPLM (one round) will be: $\phi_1 \circ \psi(\mathbf{X})$; Otherwise, the two rounds of FPLM is: $\phi_2 \circ \phi_1 \circ \psi(\mathbf{X})$.

D. one-to-one mapping induced from FPLM on triangulation

Proposition 4. *FPLM maps all non-fixed points inside the convex hull formed by the fixed points ($\mathbf{P}(\mathbf{C})$).*

Proof. From previous discussion, it is clear that FPLM is a convex combination mapping, meaning every non-fixed point must be a convex combination of its neighbors. Assuming on contrary, there is one point outside the convex hull of $\mathbf{P}(\mathbf{C})$, then there must be more points outside too due to (4). For those outside points, find the one on the edge of the convex hull (this point always exists due to finiteness), then it must have more points surrounding it too. Continue this process until all non-fixed points are exhausted. The out-most one will not have a convex hull formed by its neighbors according to supporting hyperplane theorem [26]. This is against the fact that every non-fixed point has to be convex combination of its neighbors. Therefore the assumption is incorrect. \square

We now restrict to 2-manifolds and prove that the mappings induced by both two rounds of FPLM are one-to-one over triangulation, followed by the work from [20], we firstly state the Radó-Kneser-Choquet theorem (RKC):

Theorem 4 (Radó-Kneser-Choquet). *Suppose \mathcal{T} is a strongly connected triangulation and that $\phi : D_{\mathcal{T}} \rightarrow \mathbb{R}^2$ is a convex combination mapping which maps $\partial D_{\mathcal{T}}$ homeomorphically into the boundary $\partial\Omega$ of some (closed) convex region $\Omega \subset \mathbb{R}^2$. Then ϕ is one-to-one.*

By generalizing the RKC theorem, Floater's [20] work provided a necessary and sufficient one-to-one condition of ϕ for any triangulation:

Theorem 5 (Floater, 2003). *Suppose \mathcal{T} is any triangulation and let $\phi : D_{\mathcal{T}} \rightarrow \mathbb{R}^2$ is a convex combination mapping which maps $\partial D_{\mathcal{T}}$ homeomorphically into the boundary $\partial\Omega$ of some (closed) convex region $\Omega \subset \mathbb{R}^2$. Then ϕ is one-to-one if and only if no dividing edge $[v, w]$ of \mathcal{T} is mapped by ϕ into $\partial\Omega$.*

Followed by the above claims, we now explore the features of ϕ_1 which is the induced mapping from the first round of FPLM.

Proposition 5. *If \mathcal{T} is strongly connected, then $\mathbf{P}(\mathbf{C}_2)$ must be a convex polygon formed by the boundary vertices of \mathcal{T} .*

Proof. We first identify that all points in \mathbf{C}_2 are boundary points of the 2-manifold \mathcal{M} . The boundary of the manifold forms a closed sub-manifold of dimension 1, which is reflected as the boundary points of \mathcal{T} a closed polygon homeomorphic to S^1 , i.e. $\mathbf{P}(\mathbf{C}_2)$. Assume that there is at least one vertex inside $\mathbf{P}(\mathbf{C}_2)$. Applying Theorem 1 with Tutte's spring embedding theorem [19], and combining the fact that a triangle is a convex body of dimension 2, one can draw the planar graph on \mathbb{R}^2 without edge cross. The point inside $\mathbf{P}(\mathbf{C}_2)$ must connect to fixed points via edges as manifold is connected. Therefore there must be edge cross, which is against the no edge cross assertion, and hence there is no point inside $\mathbf{P}(\mathbf{C}_2)$.

Next we show $\mathbf{P}(\mathbf{C}_2)$ is convex. Assume that $\mathbf{P}(\mathbf{C}_2)$ is concave and vertex p is the intersection of the inward edges. Due to the fact that \mathbf{C}_2 are boundary points, and there is no point inside $\mathbf{P}(\mathbf{C}_2)$, one can place a line (supporting line of convex shape) such that p 's direct neighbors including the non-boundary points and 2 boundary points that are directly connected to p , are on one side of the line. This contradicts to (12) and therefore $\mathbf{P}(\mathbf{C}_2)$ must be convex. \square

Proposition 6. *If \mathcal{T} is strongly connected. The mapping ϕ_1 induced from the first round of FPLM is one-to-one.*

Proof. The result is directly from Theorem 5 as a triangle is a convex hull in \mathbb{R}^2 and without any dividing edge across the triangle. \square

We now explore the property of the second round of FPLM. Recall that the second round of FPLM takes the simple polygon formed by joining the boundary vertices inside the first round FPLM result.

Lemma 3. *Given a strongly connected \mathcal{T}' , the mapping of second round of FPLM bounded by the convex polygon $\mathbf{P}(\mathbf{C}_2)$ is one-to-one.*

Proof. Given $\mathbf{P}(\mathbf{C}_2)$ is a convex polygon without dividing edge due to Proposition 5, the one-to-one result is obvious combining Theorem 5. \square

Remark 3 (Special case of the first round of FPLM). *When the triangulation is not strongly connected, the first round of FPLM is no longer injective because the dividing edge forms a closed boundary of a subset of the manifold causing the part of the manifold that does not contain the selected triangle to collapse into the dividing edge. Therefore, we have to directly detect the boundary from \mathcal{G}_S and generate a p-side convex polygon in \mathbb{R}^2 so that all dividing edges remain inside the boundary and none of the boundary vertices are colinear. Theorem 5 leads to Theorem 2 directly and justifies our choice.*

From the lemma above, we know that given a strongly connected triangulation \mathcal{T} on the manifold, \mathcal{T} can be mapped into a closed convex subset in \mathbb{R}^2 by using either one or two rounds of FPLM.

Remark 4 (Manifold with genus). *For surface manifolds, the genus of them is an integer (g) representing the maximum number of cuttings along non-intersecting closed simple curves without rendering the resultant manifold disconnected [44]. It will interfere with the boundary detection on the manifold compromising boundary identifiability. Hence FPLM is not functional to the surface manifold with non-zero genus such as torus.*

Remark 5 (Bijectivity and Homeomorphism). *The sample $\mathbf{X} = \{\mathbf{x}_1, \mathbf{x}_2, \dots, \mathbf{x}_N\}$ we observed is a subset of a manifold. Since the FPLM maps the triangulation \mathcal{T} on the 2-manifold to a convex closed area in \mathbb{R}^2 , and every 2, 1, 0-simplex in \mathcal{T} is mapped to exactly one specific 2, 1, 0-simplex in \mathbb{R}^2 , together with the chart map, the mapping induced from FPLM*

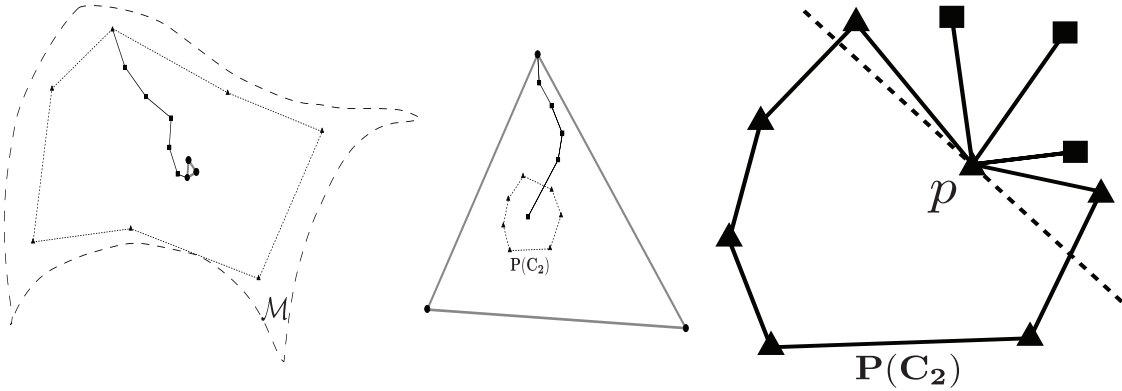


Fig. 11. Illustration of the proof. 1. No point inside $P(C_2)$; 2. Convexity of $P(C_2)$

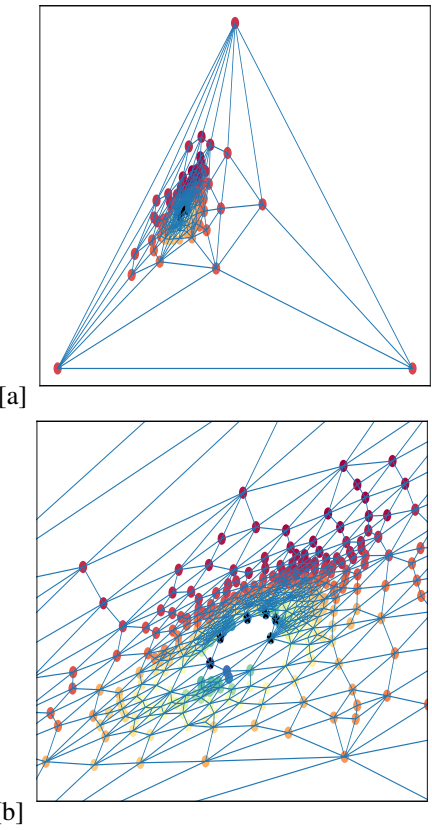


Fig. 12. The convex polygon (Vertices shown as black stars) formed by the boundary points from strongly connected triangulation.

(i.e. $\phi_1 \circ \psi$ for one round, $\phi_2 \circ \phi_1 \circ \psi$ for two rounds) is at least continuous over T and one-to-one. Hence, the mapping generated by Algorithm 1 process ($\phi \circ \psi$) restricted to a closed area in \mathbb{R}^2 is bijective.

Based on the property of FPLM on 2-manifolds, we now explore the feature of FPLM when the manifold structure is obtained by edge-to-edge tessellation of polygons (triangle is a three-sided polygon).

Definition 5 (Edge-to-Edge polygons Tessellation on 2-manifolds). *Given 2-manifold, if the manifold can be decomposed with a list of polygons with the number of side (n) larger than equal to 3, and the intersection between each polygon can only either be empty, a common point, or a common edge, we then say this manifold is tessellated by these polygons, and that is an edge-to-edge tessellation on the manifold.*

Let \mathcal{TL} be the tessellation described above. If we further triangulate \mathcal{TL} , for example we add edges which partition each face of \mathcal{TL} into triangles, then we can use convex combination mapping $\phi' : D_{\mathcal{TL}} \rightarrow \mathbb{R}^2$ and the ϕ' is linear over each triangle in $D_{\mathcal{TL}}$ and continuous. Clearly, if \mathcal{TL} is strongly connected, based what we discussed earlier, Algorithm 1 is one-to-one with the requirement that the selected polygon in the first round is convex. If \mathcal{TL} is not strongly connected, again, boundary detection is necessary to form a p side polygon manually.

We now focus on the property of FPLM in higher dimensional simplex decomposition. Taking 3-simplex decomposition (tetrahedralization) as an example, it has been reported that the convex combination mapping may not be one-to-one over tetrahedral meshes, and a counter-example has been reported in [35]. However, the counter-example mentioned on that paper has four points positioned in one face of a tetrahedron, this conflicts our assumption that all points should in general position. Also as FPLM starts from sum of squared distances, which corresponding to a special type of convex mapping, different from the one in [35]. Hence, FPLM still works for this counter example.

In regards to d -manifold for $d > 2$, the situation is more complicated. The bijectivity of piece-wise linear mapping relates to orientation preserving and some boundary conditions. We restate the key theorem here, which is in [36].

Theorem 6 (Sufficient conditions for bijectivity). *Given a d dimensional connected orientable manifold \mathcal{M} and its d -simplex decomposition constructed on a discrete sample, then a piece-wise linear mapping ϕ from \mathcal{M} to \mathbb{R}^d is bijective if it satisfies the following conditions :*

- 1) *The mapping ϕ is orientation preserving over entire*

decomposition.

- 2) The boundary of simplex decomposition is mapped to a polytope in \mathbb{R}^d bijectively.

The first round FPLM with a selected simplex maps the boundary of the manifold in the centre of the simplex as a convex polytope as shown in 5. This step guarantees the second condition mentioned above. However, orientation preserving property is not yet clarified, although we conjure that it may be there. The experiments of 3-manifolds support this conjecture. Therefore rigorous proof is still wanted.

In this section, we add more experimental results and briefly introduce the d-simplex decomposition methods such as Tangential Complex and Tetgen.

Tangential Complex

Followed by [24], we use the Tangential Complex (TC) algorithm to construct triangulation on the manifold. One requirement for conducting TC is to require that each point's tangent space on the manifold be estimated by using PCA. The tangential complex is obtained by gluing the local (Delaunay) triangulations around each sample point. The output of TC is a sub-complex of the l -dimensional Delaunay simplices of the sample points, but it can be computed using mostly operations in the d -dimensional tangent spaces. [24]. It can be proved that the output of the reconstructed manifold from the TC algorithm can be isotopic to the original manifold. However, due to the appearance of so-called *inconsistencies*, TC does not always generate the triangulation result that we defined in II-B. Even though this situation has been reported [45], there is no universal solution except for the case of curves ($d = 1$) [46]. Hence, one way to deal with this problem is to give each point that contained inconsistent simplex a small perturbation of their weights so that the position of *medial axis* of the points can be adjusted accordingly. Unfortunately, there is no guarantee that this perturbation method can always reduce the number of inconsistencies to zero. Hence, if the TC result has inconsistency even after perturbation, we will use Delaunay or surface triangulation.

Tetgen

One of the most widely applied tetrahedral mesh generation methods: Tetgen, is comprehensively described in [37]. It is a mixture of a few classic constrain methods described in [47] and the classic Delaunay refinement algorithm [48]. Given a set of points from an underlying manifold in \mathbb{R}^l , with an intrinsic dimension equal to three, Tetgen can generate a 3D piece-wise linear complex, collectively named as cells. The property of such cells includes 1. the boundary of each cell in the complex is a union of cells in the complex; 2. The intersection (if it exists) of two cells is the simplicial complex with a lower dimension, at least less than one compared to the two intersected cells. If all the cells in these underlying 3-manifolds are tetrahedral, we would call the piece-wise linear complex formed by tetrahedral mesh. More generally, the piece-wise linear meshes generated from Tetgen offer a facet-to-facet tessellation of manifold in \mathbb{R}^l .

E. Additional results on 2-manifolds

We add some additional experimental results for 2-manifolds including: Monkey Saddle, Paraboloid, Twinpeaks and Sphere. A summary of all manifolds included in the experiment and the number of line crosses generated from the methods other than FPLM are included in table I.

F. Additional result on tetrahedral meshes

We additionally provide this result to show that FPLM can deal with large number of tetrahedral mesh in \mathbb{R}^3 . Note that the boundary of manifold (i.e. in \mathbb{R}^4 or higher) will generally be different compared with the boundary detected in \mathbb{R}^3 , since there are many types of embedding functions to map 3 dimensional tetrahedral mesh into \mathbb{R}^4 . We select the famous SHARK tetrahedral mesh [39] that contains 17061 tetrahedrons to check the efficiency of FPLM. The results are as follows:

G. Effect of noise on paraboloid data

To evaluate the robustness to noised samples, we inject some random Gaussian noise to the z-values, i.e. $z = f(x, y) = x^2 + y^2 + \epsilon$, where $\epsilon \sim \mathcal{N}(0, \sigma)$. We test on three levels of noise variance, $\sigma = 0.001, 0.005, 0.01$ and the mapping results are shown in Fig. 22. We observe that when the noise level is relatively small ($\sigma = 0.001$), the simplex decomposition generated by TC is still valid and hence FPLM can guarantee a valid mapping. When the noise level increases, we see TC fails to generate a valid decomposition and thus, FPLM fails to preserve the bijectivity. From the theoretical analysis in this paper, as long as the simplex decomposition is valid, FPLM is guaranteed to succeed regardless of the noise level.

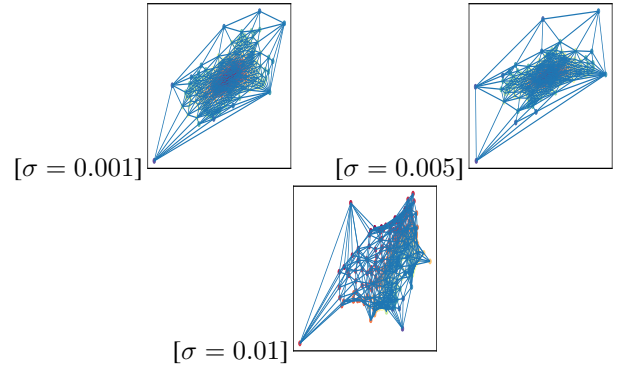


Fig. 22. Result on noise-injected paraboloid samples. The number of crosses are (a) 0, (b) 14, (c) 2108.

TABLE I

SUMMARY OF LINE CROSSES FOR MULTIPLE MANIFOLD DATASETS VIA DIFFERENT LEARNING ALGORITHMS. IT IS CLEAR THAT ALL INCLUDED METHODS SUFFER FROM LARGE NUMBER OF LINE CROSSES AND THUS RESULTING A POTENTIAL ISSUE OF IN-DISTINGUISHABILITY. WE NOTE THAT THE NUMBER OF LINE CROSSES FOR OUR METHOD (FPLM) IS 0 FOR ALL DATASETS

Manifolds	Methods and Line crosses						
	Autoencoder	Isomap	LE	LLE	LTSA	MDS	TSNE
Monkey Saddle	54	46	815	57	33	47	735
Swiss Roll	4585	1942	937	3623	36773	3804	10088
Sphere	770	1786	1683	1883	1795	1667	2329
Twin Peaks	100	114	903	2806	696	91	235
Paraboloid	56	39	1468	309	309	38	282

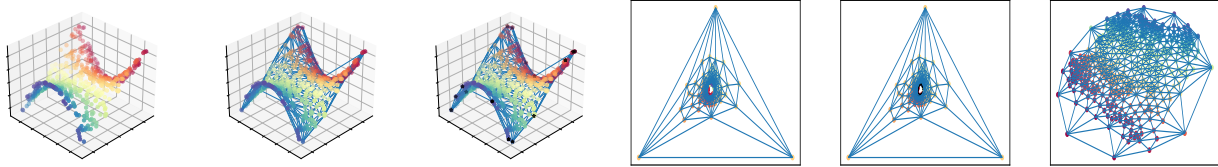


Fig. 13. FPLM on Monkey Saddle, (a) Manifold scatters,(b) Triangulation on manifold, (c) Boundary detection from triangulation result, (d) First round FPLM result, (e) Boundary detection of the first round FPLM, (f) Final result.

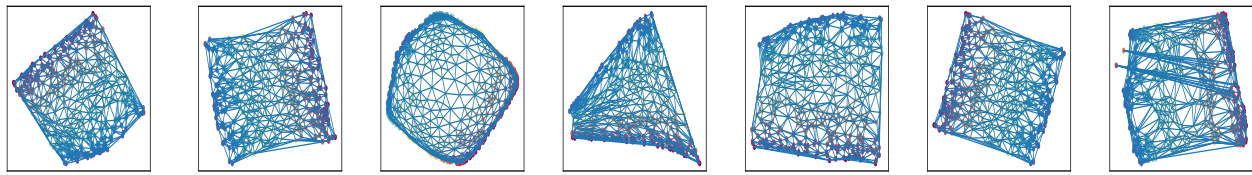


Fig. 14. Other methods on monkey saddle. AE: 21 crosses, Isomap: 46 crosses, LE: 815 crosses, LLE: 57 cross, LTSA 33 crosses, (f) 41 crosses, t-SNE 735 crosses

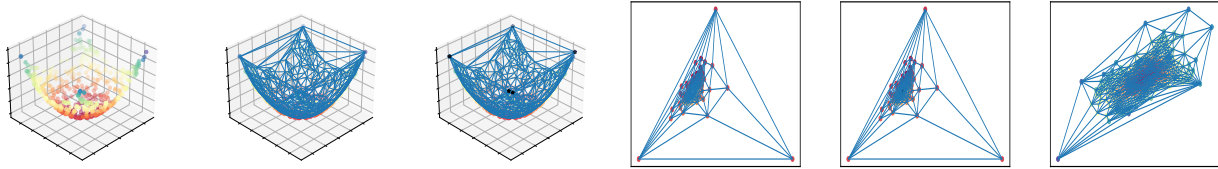


Fig. 15. FPLM on Paraboloid, (a) Manifold scatters,(b) Triangulation on manifold, (c) Boundary detection from triangulation result, (d) First round FPLM result, (e) Boundary detection of the first round FPLM, (f) Final result.

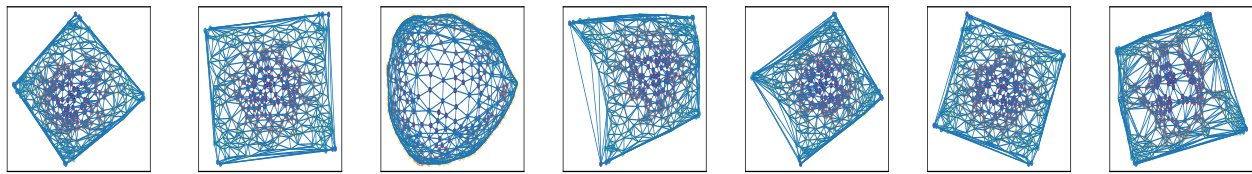


Fig. 16. Other methods on Paraboloid: AE: 122 crosses, Isomap 39 crosses, LE: 1468 crosses, LLE: 309 cross, LTSA: 30 crosses, MDS: 57 crosses, t-SNE 282 crosses

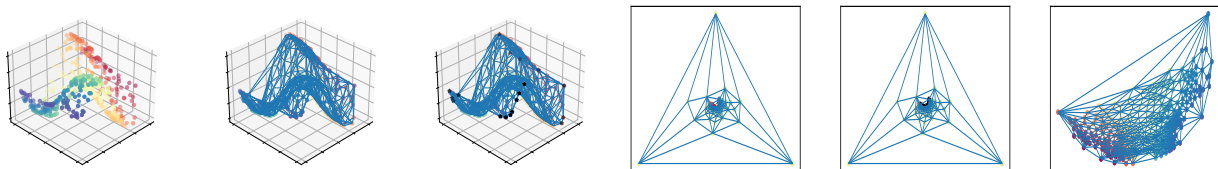


Fig. 17. FPLM on Twinpeaks

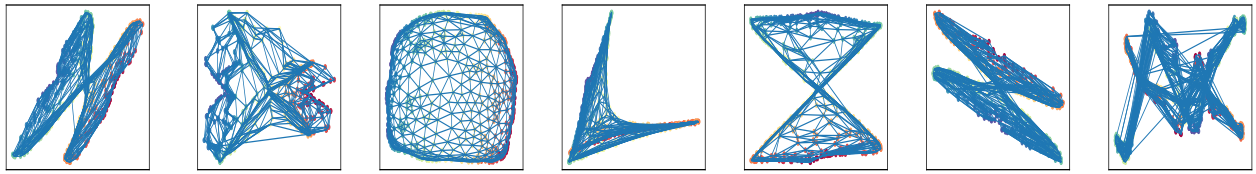


Fig. 18. Other methods on Twinpeaks: AE: 3332 crosses, Isomap: 964 crosses, LE: 764 crosses, LLE: 3751 cross, LTSA: 2976 crosses, MDS: 3584 crosses, t-SNE 18282 crosses

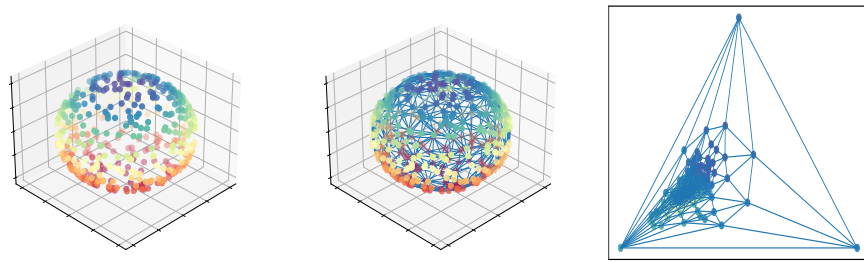


Fig. 19. FPLM on Sphere

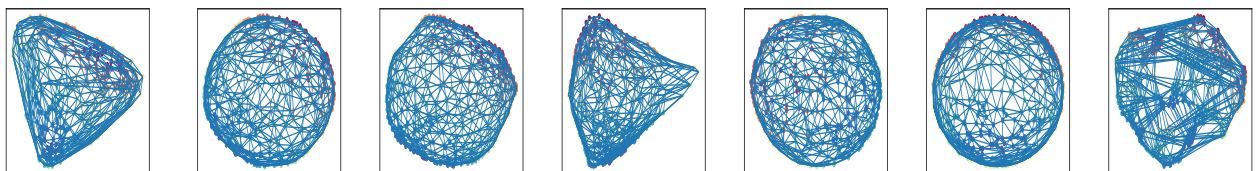


Fig. 20. Other methods on Sphere. AE: 770 crosses, Isomap: 1786 crosses, LE: 1683 crosses, LLE: 1883 cross, LTSA: 1795 crosses, MDS: 1667 crosses, t-SNE 2329 crosses

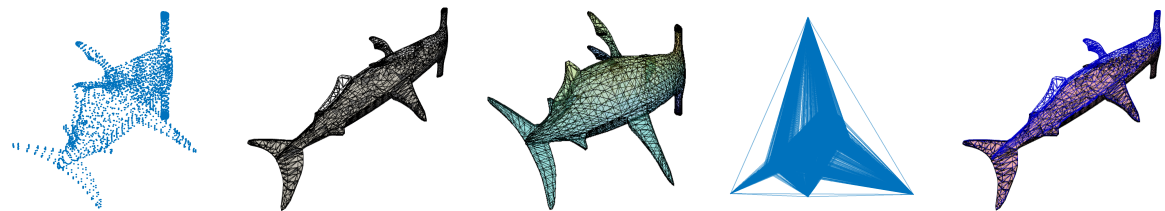


Fig. 21. FPLM on shark sharp manifold example: 1. Point scatter 2. tetrahedralization on scatters 3. Boundary detection (faces) 4. First round FPLM 5. Second round FPLM. Total running time: 38.5s